CHAPTER – 8

DENSITY FUNCTIONAL THEORY STUDIES ON THE MOLECULAR STRUCTURE, SPECTRA (FT-IR, FT-RAMAN AND UV) AND NBO ANALYSIS OF ETHYL CENTRALITE

The organic compound 1, 3-diethyl-1, 3-diphenylurea commonly known as ethyl centralite, carbamite or centralite No. 1 is a derivative of urea, used as the gelatinizing agent in smokeless powder [151]. Ethyl centralite (EC) was used as a stabilizer to prevent slow decomposition of nitrocellulose in propellants [152, 153]. EC is used as an additive in solid rocket propellants in addition to its use in smokeless gun-powders [154]. Ethyl centralite is a deterrent used as a burn rate moderator which increases the shelf life of the propellant [155]. EC is considered as highly credible organic gunshot residue and accurate analysis of which is of value to forensic scientists [156]. In the crystalline state of ethyl centralite, intermolecular C–H···O hydrogen bonds gives rise to centrosymmetric dimer [157].

Spectroscopic studies of various diphenyl compounds like 1, 3-diphenylurea have been analyzed and reported [19]. This work deals with the spectroscopic analysis of EC using FT-IR, FT-Raman and UV-visible spectra to expound the molecular structure, hyperconjugation interaction and non linear optical properties of the compound supported by density functional theory (DFT) and time dependent density functional theory (TD-DFT) calculations. Vibrational assignments of EC have been made using the scaled quantum mechanical (SQM) force field technique.

8.1 Experimental details

The compound ethyl centralite was purchased from Sigma-Aldrich with 99% purity and used without further purification. The Fourier transform infrared and Raman spectra have been recorded in the region 4000 – 400 cm^{-1} and 3500 – 50 cm^{-1}

using diffuse reflectance method with the Jasco FT/IR-6300 and FT-Raman Bruker RFS 100/S instrument respectively. The resolution of both the spectrum was 4 cm^{-1}. An air cooled Nd:YAG laser of 1064nm wavelength and 150mW laser power was used as the exciting source. The standard Germanium was used as the detector. The UV-visible spectrum of EC was recorded in ethanol solution using a Cary 5E UV-VIS-NIR spectrophotometer.

8.2 Optimized geometries

The optimized molecular structure of EC calculated using Gaussian 09 program is shown in Fig. 8.1. The optimized geometry agrees well with the experimental geometry showing that the geometry optimization almost exactly reproduces the experimental structure. A small discrepancy in the computed parameters from the XRD data is due to the ignorance of intermolecular interaction in the calculations.

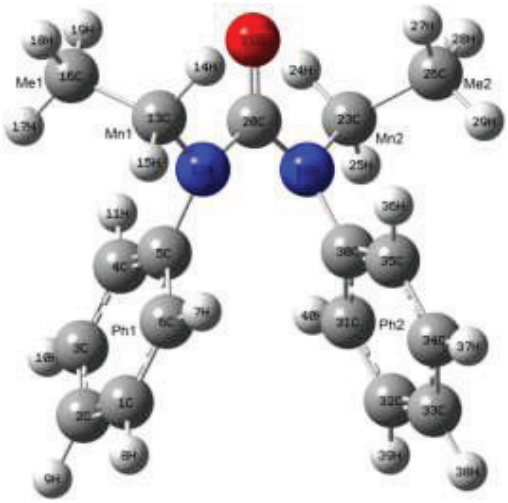

Fig. 8.1 Optimized molecular structure of ethyl centralite.

The optimized geometrical parameters are given in Tables 8.1 and 8.2 with the comparison of experimental data [157]. In both the phenyl rings, the C−C bonds

(C_4–C_5, C_5–C_6, C_{30}–C_{31} and C_{30}–C_{35}) on either side of urea moiety are equal to 1.40Å whereas other C–C bonds range from 1.394 – 1.396Å. The ring loses its symmetry owing to strong phenyl-N conjugation between nitrogen lone pair electrons and the phenyl ring π-system. The slight reduction of endocyclic angles C_4–C_5–C_6 and C_{31}–C_{30}–C_{35} of phenyl rings (I and II) by 0.78˚ is due to phenyl-N conjugation. The other endocyclic angles remain ~120˚ satisfying the typical hexagonal angle. The non-planarity of the phenyl rings is evident from the dihedral angles C_2–C_3–C_4–C_5, C_{33}–C_{34}–C_{35}–C_{30} (1.14°) and C_3–C_4–C_5–C_6, C_{31}–C_{30}–C_{35}–C_{34} (−0.91°). The dihedral angles of C_{13}–N_{12}–C_{20}–O_{21} (−9.87°), C_{13}–N_{12}–C_{20}–N_{22} (170.12°) and O_{21}–C_{20}–N_{22}–C_{23} (−9.87°), N_{12}–C_{20}–N_{22}–C_{23} (170.14°) indicates that the urea moiety is non-planar. The two phenyl rings were not coplanar with the urea moiety, which is evident from the dihedral angles of C_6–C_5–N_{12}–C_{20} (137.36°) and C_{20}–N_{22}–C_{30}–C_{31} (137.31°).

Table 8.1 Selected bond lengths and bond angles of ethyl centralite by B3LYP/6-31G(d) in comparison with the XRD data.

Bond length			Bond angle		
Parameter	**Calc. (Å)**	**Expt. [157] (Å)**	**Parameter**	**Calc. (°)**	**Expt. [157] (°)**
C_1–C_2	1.396	1.379	C_2–C_1–C_6	120.31	120.51
C_1–C_6	1.394	1.382	C_1–C_2–C_3	119.52	119.96
C_1–H_8	1.087	0.950	C_2–C_3–C_4	120.36	120.07
C_2–C_3	1.396	1.377	C_3–C_4–C_5	120.24	120.00
C_2–H_9	1.087	0.951	C_4–C_5–C_6	119.22	119.71
C_3–C_4	1.395	1.385	C_4–C_5–N_{12}	121.09	120.96
C_3–H_{10}	1.087	0.950	C_6–C_5–N_{12}	119.63	119.17
C_4–C_5	1.401	1.389	C_1–C_6–C_5	120.35	119.73
C_4–H_{11}	1.086	0.951	C_5–N_{12}–C_{13}	116.72	115.12

Bond length			Bond angle		
Parameter	**Calc. (Å)**	**Expt. [157] (Å)**	**Parameter**	**Calc. (°)**	**Expt. [157] (°)**
C_5–C_6	1.400	1.386	C_5–N_{12}–C_{20}	122.95	123.66
C_5–N_{12}	1.432	1.431	C_{13}–N_{12}–C_{20}	115.84	116.50
C_6–H_7	1.086	0.950	N_{12}–C_{13}–H_{14}	107.08	109.01
N_{12}–C_{13}	1.477	1.470	N_{12}–C_{13}–H_{15}	107.17	108.96
N_{12}–C_{20}	1.395	1.380	N_{12}–C_{13}–C_{16}	113.90	112.98
C_{13}–H_{14}	1.092	0.990	H_{14}–C_{13}–C_{16}	110.03	108.99
C_{13}–H_{15}	1.095	0.990	H_{15}–C_{13}–C_{16}	110.42	108.98
C_{13}–C_{16}	1.530	1.508	C_{13}–C_{16}–H_{17}	111.24	109.43
C_{16}–H_{17}	1.096	0.980	C_{13}–C_{16}–H_{18}	110.07	109.50
C_{16}–H_{18}	1.097	0.979	C_{13}–C_{16}–H_{19}	109.99	109.44
C_{16}–H_{19}	1.093	0.980	H_{17}–C_{16}–H_{18}	107.98	109.51
C_{20}–O_{21}	1.230	1.227	H_{18}–C_{16}–H_{19}	108.51	109.53
C_{20}–N_{22}	1.395	1.375	N_{12}–C_{20}–O_{21}	121.66	121.24
N_{22}–C_{23}	1.477	1.473	N_{12}–C_{20}–N_{22}	116.69	117.25
N_{22}–C_{30}	1.432	1.435	O_{21}–C_{20}–N_{22}	121.65	121.51
C_{23}–H_{24}	1.092	0.991	C_{20}–N_{22}–C_{23}	115.84	116.15
C_{23}–H_{25}	1.095	0.990	C_{20}–N_{22}–C_{30}	122.97	123.78
C_{23}–C_{26}	1.530	1.513	C_{23}–N_{22}–C_{30}	116.73	115.17
C_{26}–H_{27}	1.093	0.980	N_{22}–C_{23}–H_{24}	107.08	109.10
C_{26}–H_{28}	1.097	0.980	N_{22}–C_{23}–H_{25}	107.18	109.11
C_{26}–H_{29}	1.096	0.980	N_{22}–C_{23}–C_{26}	113.89	112.52
C_{30}–C_{31}	1.400	1.382	H_{24}–C_{23}–C_{26}	110.03	109.09
C_{30}–C_{35}	1.401	1.390	H_{25}–C_{23}–C_{26}	110.42	109.07
C_{31}–C_{32}	1.394	1.384	C_{23}–C_{26}–H_{27}	109.99	109.46
C_{31}–H_{40}	1.086	0.950	C_{23}–C_{26}–H_{28}	110.07	109.47
C_{32}–C_{33}	1.396	1.385	C_{23}–C_{26}–H_{29}	111.24	109.46
C_{32}–H_{39}	1.087	0.950	H_{27}–C_{26}–H_{28}	108.50	109.52

Bond length			Bond angle		
Parameter	**Calc. (Å)**	**Expt. [157] (Å)**	**Parameter**	**Calc. (°)**	**Expt. [157] (°)**
$C_{33}–C_{34}$	1.396	1.378	$H_{28}–C_{26}–H_{29}$	107.98	109.48
$C_{33}–H_{38}$	1.087	0.951	$N_{22}–C_{30}–C_{31}$	119.64	118.95
$C_{34}–C_{35}$	1.395	1.384	$N_{22}–C_{30}–C_{35}$	121.08	120.89
$C_{34}–H_{37}$	1.087	0.950	$C_{31}–C_{30}–C_{35}$	119.22	120.02
$C_{35}–H_{36}$	1.086	0.950	$C_{30}–C_{31}–C_{32}$	120.35	119.91
-	-	-	$C_{31}–C_{32}–C_{33}$	120.31	120.08
-	-	-	$C_{32}–C_{33}–C_{34}$	119.52	120.00
-	-	-	$C_{33}–C_{34}–C_{35}$	120.36	120.23
-	-	-	$C_{30}–C_{35}–C_{34}$	120.24	119.75

Table 8.2 Dihedral angles of ethyl centralite by B3LYP/6-31G(d) in comparison with the XRD data.

Dihedral angle		
Parameter	**Calc. (°)**	**Expt. [157] (°)**
$C_6–C_1–C_2–C_3$	-0.43	-0.09
$C_6–C_1–C_2–H_9$	179.60	179.87
$H_8–C_1–C_2–C_3$	-179.62	179.92
$H_8–C_1–C_2–H_9$	0.40	-0.11
$C_2–C_1–C_6–C_5$	0.66	0.73
$C_2–C_1–C_6–H_7$	-178.35	-179.26
$H_8–C_1–C_6–C_5$	179.85	-179.28
$H_8–C_1–C_6–H_7$	0.84	0.72
$C_1–C_2–C_3–C_4$	-0.46	-1.03
$C_1–C_2–C_3–H_{10}$	-179.46	178.96
$H_9–C_2–C_3–C_4$	179.51	179.00
$H_9–C_2–C_3–H_{10}$	0.52	-1.00
$C_2–C_3–C_4–C_5$	1.14	1.51
$C_2–C_3–C_4–H_{11}$	-178.94	-178.52
$H_{10}–C_3–C_4–C_5$	-179.86	-178.49
$H_{10}–C_3–C_4–H_{11}$	0.06	1.48
$C_3–C_4–C_5–C_6$	-0.91	-0.86

Dihedral angle		
Parameter	**Calc. (°)**	**Expt. [157] (°)**
C_3–C_4–C_5–N_{12}	-178.12	-176.14
H_{11}–C_4–C_5–C_6	179.17	179.17
H_{11}–C_4–C_5–N_{12}	1.96	3.88
C_4–C_5–C_6–C_1	0.02	-0.26
C_4–C_5–C_6–H_7	179.04	179.74
N_{12}–C_5–C_6–C_1	177.26	175.11
N_{12}–C_5–C_6–H_7	-3.72	-4.89
C_4–C_5–N_{12}–C_{13}	109.75	108.86
C_4–C_5–N_{12}–C_{20}	-45.45	-45.85
C_6–C_5–N_{12}–C_{13}	-67.45	-66.45
C_6–C_5–N_{12}–C_{20}	137.36	138.84
C_5–N_{12}–C_{13}–H_{14}	164.64	171.52
C_5–N_{12}–C_{13}–H_{15}	48.96	54.12
C_5–N_{12}–C_{13}–C_{16}	-73.48	-67.15
C_{20}–N_{12}–C_{13}–H_{14}	-38.38	-31.89
C_{20}–N_{12}–C_{13}–H_{15}	-154.06	-149.29
C_{20}–N_{12}–C_{13}–C_{16}	83.50	89.43
C_5–N_{12}–C_{20}–O_{21}	145.53	150.16
C_5–N_{12}–C_{20}–N_{22}	-34.48	-29.74
C_{13}–N_{12}–C_{20}–O_{21}	-9.87	-4.23
C_{13}–N_{12}–C_{20}–N_{22}	170.12	175.87
N_{12}–C_{13}–C_{16}–H_{17}	58.88	60.93
N_{12}–C_{13}–C_{16}–H_{18}	178.52	-179.28
N_{12}–C_{13}–C_{16}–H_{19}	-61.98	-58.96
H_{14}–C_{13}–C_{16}–H_{17}	179.12	-177.72
H_{14}–C_{13}–C_{16}–H_{18}	-61.24	-57.69
H_{14}–C_{13}–C_{16}–H_{19}	58.26	62.38
H_{15}–C_{13}–C_{16}–H_{17}	-61.76	-60.34
H_{15}–C_{13}–C_{16}–H_{18}	57.88	59.70
H_{15}–C_{13}–C_{16}–H_{19}	177.39	179.77
N_{12}–C_{20}–N_{22}–C_{23}	170.14	175.84
N_{12}–C_{20}–N_{22}–C_{30}	-34.39	-30.20
O_{21}–C_{20}–N_{22}–C_{23}	-9.87	-4.07

Dihedral angle		
Parameter	**Calc. (°)**	**Expt. [157] (°)**
$O_{21}–C_{20}–N_{22}–C_{30}$	145.60	149.90
$C_{20}–N_{22}–C_{23}–H_{24}$	-38.35	-36.02
$C_{20}–N_{22}–C_{23}–H_{25}$	-154.04	-153.62
$C_{20}–N_{22}–C_{23}–C_{26}$	83.52	85.19
$C_{30}–N_{22}–C_{23}–H_{24}$	164.60	167.74
$C_{30}–N_{22}–C_{23}–H_{25}$	48.91	50.15
$C_{30}–N_{22}–C_{23}–C_{26}$	-73.53	-71.04
$C_{20}–N_{22}–C_{30}–C_{31}$	137.31	136.14
$C_{20}–N_{22}–C_{30}–C_{35}$	-45.49	-48.08
$C_{23}–N_{22}–C_{30}–C_{31}$	-67.42	-69.66
$C_{23}–N_{22}–C_{30}–C_{35}$	109.78	106.12
$N_{22}–C_{23}–C_{26}–H_{27}$	-61.98	-58.82
$N_{22}–C_{23}–C_{26}–H_{28}$	178.51	-178.82
$N_{22}–C_{23}–C_{26}–H_{29}$	58.87	61.14
$H_{24}–C_{23}–C_{26}–H_{27}$	58.25	62.39
$H_{24}–C_{23}–C_{26}–H_{28}$	-61.25	-57.60
$H_{24}–C_{23}–C_{26}–H_{29}$	179.10	-177.65
$H_{25}–C_{23}–C_{26}–H_{27}$	177.38	179.97
$H_{25}–C_{23}–C_{26}–H_{28}$	57.87	59.97
$H_{25}–C_{23}–C_{26}–H_{29}$	-61.77	-60.08
$N_{22}–C_{30}–C_{31}–C_{32}$	177.26	176.32
$N_{22}–C_{30}–C_{31}–H_{40}$	-3.72	-3.65
$C_{35}–C_{30}–C_{31}–C_{32}$	0.02	0.51
$C_{35}–C_{30}–C_{31}–H_{40}$	179.04	-179.46
$N_{22}–C_{30}–C_{35}–C_{34}$	-178.12	-176.53
$N_{22}–C_{30}–C_{35}–H_{36}$	1.96	3.51
$C_{31}–C_{30}–C_{35}–C_{34}$	-0.91	-0.80
$C_{31}–C_{30}–C_{35}–H_{36}$	179.17	179.24
$C_{30}–C_{31}–C_{32}–C_{33}$	0.66	-0.06
$C_{30}–C_{31}–C_{32}–H_{39}$	179.85	-179.99
$H_{40}–C_{31}–C_{32}–C_{33}$	-178.35	179.91
$H_{40}–C_{31}–C_{32}–H_{39}$	0.84	-0.02
$C_{31}–C_{32}–C_{33}–C_{34}$	-0.43	-0.10
$C_{31}–C_{32}–C_{33}–H_{38}$	179.60	179.85

Dihedral angle		
Parameter	**Calc. (°)**	**Expt. [157] (°)**
H_{39}–C_{32}–C_{33}–C_{34}	-179.62	179.83
H_{39}–C_{32}–C_{33}–H_{38}	0.40	-0.22
C_{32}–C_{33}–C_{34}–C_{35}	-0.46	-0.19
C_{32}–C_{33}–C_{34}–H_{37}	-179.45	179.84
H_{38}–C_{33}–C_{34}–C_{35}	179.51	179.86
H_{38}–C_{33}–C_{34}–H_{37}	0.52	-0.11
C_{33}–C_{34}–C_{35}–C_{30}	1.14	0.64
C_{33}–C_{34}–C_{35}–H_{36}	-178.94	-179.40
H_{37}–C_{34}–C_{35}–C_{30}	-179.86	-179.39
H_{37}–C_{34}–C_{35}–H_{36}	0.06	0.57

8.3 Natural bond orbital analysis

The donor-acceptor orbital interaction with the interaction energies and the electron densities calculated by the second order perturbation theory analysis of Fock matrix in the NBO basis are summarized in Table 8.3. The intramolecular hyperconjugative interactions in EC were formed by the orbital overlap between $\pi(C_1–C_6)$ and $\pi^*(C_2–C_3)$, $\pi^*(C_4–C_5)$ resulting in the stabilization energy of 19.77 and 20.83 kcalmol^{-1} respectively. Similar orbital overlaps between π(C–C) and geminal π^*(C–C) bond orbitals of both the phenyl rings (Ph1, Ph2) with high energy are listed in Table 2. The $n_1(N_{12})\rightarrow\sigma^*(C_4–C_5)$/ $\sigma^*(C_5–C_6)$ and $n_1(N_{22})\rightarrow\sigma^*(C_{30}–C_{31})$/ $\sigma^*(C_{30}–C_{35})$ delocalization on both the phenyl rings of energy 5.77/3.50 kcalmol^{-1} is responsible for lengthening the bonds ($C_4–C_5$, $C_5–C_6$, $C_{30}–C_{31}$ and $C_{30}–C_{35}$) when compared to other bond distances in both the rings. The hyperconjugative interaction ($n\rightarrow\sigma^*$) between $n_2(O_{21})$ and antibonding acceptor orbitals ($N_{12}–C_{20}$ and $C_{20}–N_{22}$) gives rise to the stabilization energy of 24.8 kcalmol^{-1}. The most energetic interaction ($n\rightarrow\pi^*$) related to the resonance in the molecule, is electron donation from the $n_1(N_{12})$ and $n_1(N_{22})$ atoms to the antibonding acceptor $\pi^*(C_{20}–O_{21})$ resulting in the maximum stabilization energy of 49.21 and 49.29 kcalmol^{-1} respectively.

Table 8.3 Second order perturbation theory analysis of Fock matrix in NBO basis

Donor NBO (i)	ED (e)	Acceptor NBO (j)	ED (e)	E(2)[a] (Kcalmol^{-1})	E(j)−E(i)[b] (a.u.)	F(i,j)[c] (a.u.)
$\pi(C_1–C_6)$	1.67018	$\pi^*(C_2–C_3)$	0.33888	19.77	0.28	0.067
		$\pi^*(C_4–C_5)$	0.36911	20.83	0.28	0.069
$\pi(C_2–C_3)$	1.66401	$\pi^*(C_1–C_6)$	0.32723	20.68	0.28	0.068
		$\pi^*(C_4–C_5)$	0.36911	20.33	0.28	0.068
$\sigma(C_4–C_5)$	1.97543	$\sigma^*(N_{12}–C_{13})$	0.02847	1.31	1.03	0.033
$\pi(C_4–C_5)$	1.65719	$\pi^*(C_1–C_6)$	0.32723	19.52	0.29	0.067
		$\pi^*(C_2–C_3)$	0.33888	20.58	0.28	0.068
		$\pi^*(C_{30}–C_{35})$	0.36911	0.81	0.28	0.014
$\sigma(C_5–C_6)$	1.97558	$\sigma^*(C_5–N_{12})$	0.03567	1.17	1.11	0.032
		$\sigma^*(N_{12}–C_{20})$	0.08274	1.92	1.14	0.042
$\sigma(C_5–N_{12})$	1.98001	$\sigma^*(N_{12}–C_{20})$	0.08274	1.30	1.20	0.036
		$\sigma^*(C_{20}–O_{21})$	0.01606	2.54	1.35	0.052
$\pi(C_{30}–C_{35})$	1.65717	$\pi^*(C_4–C_5)$	0.36911	0.81	0.28	0.014
		$\pi^*(C_{31}–C_{32})$	0.32725	19.52	0.29	0.067
		$\pi^*(C_{33}–C_{34})$	0.33889	20.58	0.28	0.068
$\pi(C_{31}–C_{32})$	1.67018	$\pi^*(C_{30}–C_{35})$	0.36911	20.83	0.28	0.069
		$\pi^*(C_{33}–C_{34})$	0.33889	19.77	0.28	0.067
$\pi(C_{33}–C_{34})$	1.66399	$\pi^*(C_{30}–C_{35})$	0.36911	20.34	0.28	0.068
		$\pi^*(C_{31}–C_{32})$	0.32725	20.68	0.28	0.068
$n_1(N_{12})$	1.73515	$\sigma^*(C_4–C_5)$	0.02744	5.77	0.81	0.065
		$\pi^*(C_4–C_5)$	0.36911	8.53	0.28	0.045
		$\sigma^*(C_5–C_6)$	0.02595	3.50	0.82	0.051
		$\sigma^*(C_{13}–C_{16})$	0.01745	7.13	0.64	0.064
		$\pi^*(C_{20}–O_{21})$	0.37218	49.21	0.26	0.104
$n_1(O_{21})$	1.97381	$\sigma^*(N_{12}–C_{20})$	0.08274	2.07	1.11	0.043
		$\sigma^*(C_{20}–N_{22})$	0.08274	2.07	1.11	0.043
$n_2(O_{21})$	1.85729	$\sigma^*(N_{12}–C_{20})$	0.08274	24.82	0.68	0.118
		$\sigma^*(C_{20}–N_{22})$	0.08274	24.81	0.68	0.118
$n_1(N_{22})$	1.73497	$\pi^*(C_{20}–O_{21})$	0.37218	49.29	0.26	0.104
		$\sigma^*(C_{23}–C_{26})$	0.01745	7.12	0.64	0.064
		$\sigma^*(C_{30}–C_{31})$	0.02596	3.51	0.82	0.051
		$\sigma^*(C_{30}–C_{35})$	0.02744	5.77	0.81	0.065
		$\pi^*(C_{30}–C_{35})$	0.36911	8.53	0.28	0.045
$\pi^*(C_{20}–O_{21})$	0.37218	$\pi^*(C_4–C_5)$	0.36911	1.01	0.02	0.006
		$\pi^*(C_{30}–C_{35})$	0.36911	1.01	0.02	0.006
$\pi^*(C_{30}–C_{35})$	0.36911	$\sigma^*(N_{22}–C_{23})$	0.02846	1.17	0.31	0.038

[a]E(2) is the energy of hyperconjugative interactions.
[b]Energy difference between donor and acceptor i and j NBO orbitals.
[c]F(i,j) is the Fock matrix element between i and j NBO orbitals.

8.4 Vibrational analysis

A complete vibrational analysis of the 114 fundamental vibrational modes of ethyl centralite has been done by normal coordinate analysis followed by scaled quantum mechanical force field calculations. Internal valence coordinates of the title compound is constructed according to Pulay's recommendations [71] and listed in Table 8.4. Force constants of the internal coordinates and the scale factors used are given in Table 8.5. Scale factors have been refined with an RMS error of 6.85 cm^{-1} between the experimental and SQM force field frequencies. The observed FT-IR and FT-Raman spectra together with the simulated spectra are shown in Fig. 8.2 and Fig. 8.3 respectively. The observed and calculated vibrational wavenumber with the PED for each normal mode are presented in Table 8.6.

Table 8.4 Definition of internal valence coordinates of ethyl centralite.

No.	Symbol	Type	Definition
		Stretching	
1–6	R_i	C-C (Ring 1)	C_1-C_2, C_2-C_3, C_3-C_4, C_4-C_5, C_5-C_6, C_6-C_1
7–11	r_i	C-H (Ring 1)	C_1-H_8, C_2-H_9, C_3-H_{10}, C_4-H_{11}, C_6-H_7
12	P_i	C-N (Ring 1)	C_5-N_{12}
13	P_i	N-C (Methylene 1)	N_{12}-C_{13}
14–15	r_i	C-H (Methylene 1)	C_{13}-H_{14}, C_{13}-H_{15}
16	r_i	C-C (Methylene 1)	C_{13}-C_{16}
17–19	ξ_i	C-H (Methyl 1)	C_{16}-H_{17}, C_{16}-H_{18}, C_{16}-H_{19}
20	Q_i	C=O	C_{20}-O_{21}
21–22	r_i	C-N (Urea)	N_{12}-C_{20}, C_{20}-N_{22}
23	P_i	N-C (Methylene 2)	N_{22}-C_{23}
24–25	r_i	C-H (Methylene 2)	C_{23}-H_{24}, C_{23}-H_{25}
26	r_i	C-C (Methylene 2)	C_{23}-C_{26}
27–29	ξ_i	C-H (Methyl 2)	C_{26}-H_{27}, C_{26}-H_{28}, C_{26}-H_{29}
30	P_i	C-N (Ring 2)	C_{30}-N_{22}
31–36	R_i	C-C (Ring 2)	C_{30}-C_{31}, C_{31}-C_{32}, C_{32}-C_{33}, C_{33}-C_{34}, C_{34}-

No.	Symbol	Type	Definition
			C_{35}, C_{35}-C_{30}
37–41	r_i	C-H (Ring 2)	C_{31}-H_{40}, C_{32}-H_{39}, C_{33}-H_{38}, C_{34}-H_{37}, C_{35}-H_{36}
Bending			
42–47	δ_i	C-C-C (Ring 1)	C_6-C_1-C_2, C_1-C_2-C_3, C_2-C_3-C_4, C_3-C_4-C_5, C_4-C_5-C_6, C_5-C_6-C_1
48–57	θ_i	H-C-C (Ring 1)	H_7-C_6-C_1, H_7-C_6-C_5, H_8-C_1-C_2, H_8-C_1-C_6, H_9-C_2-C_1, H_9-C_2-C_3, H_{10}-C_3-C_2, H_{10}-C_3-C_4, H_{11}-C_4-C_3, H_{11}-C_4-C_5
58–59	ϕ_i	N-C-C (Ring 1)	N_{12}-C_5-C_4, N_{12}-C_5-C_6
60–61	β_i	C-N-C (Ring 1)	C_5-N_{12}-C_{13}, C_5-N_{12}-C_{20}
62	α_i	C-N-C (Methylene 1)	C_{13}-N_{12}-C_{20}
63	α_i	H-C-H (Methylene 1)	H_{14}-C_{13}-H_{15}
64	γ_i	N-C-C (Methylene 1)	N_{12}-C_{13}-C_{16}
65–66	β_i	H-C-C (Methylene 1)	H_{14}-C_{13}-C_{16}, H_{15}-C_{13}-C_{16}
67–68	β_i	H-C-N (Methylene 1)	H_{14}-C_{13}-N_{12}, H_{15}-C_{13}-N_{12}
69–71	α_i	H-C-H (Methyl 1)	H_{18}-C_{16}-H_{19}, H_{17}-C_{16}-H_{19}, H_{17}-C_{16}-H_{18}
72–74	β_i	C-C-H (Methyl 1)	C_{13}-C_{16}-H_{17}, C_{13}-C_{16}-H_{18}, C_{13}-C_{16}-H_{19}
75	α_i	N-C-N (Urea)	N_{12}-C_{20}-N_{22}
76–77	β_i	N-C-O (Urea)	N_{12}-C_{20}-O_{21}, O_{21}-C_{20}-N_{22}
78–79	β_i	C-N-C (Ring 2)	C_{20}-N_{22}-C_{30}, C_{23}-N_{22}-C_{30}
80	α_i	C-N-C (Methylene 2)	C_{20}-N_{22}-C_{23}
81	α_i	H-C-H (Methylene 2)	H_{24}-C_{23}-H_{25}
82	γ_i	N-C-C (Methylene 2)	N_{22}-C_{23}-C_{26}
83–84	β_i	H-C-C (Methylene 2)	H_{24}-C_{23}-C_{26}, H_{25}-C_{23}-C_{26}
85–86	β_i	H-C-N (Methylene 2)	H_{24}-C_{23}-N_{22}, H_{25}-C_{23}-N_{22}
87–89	α_i	H-C-H (Methyl 2)	H_{28}-C_{26}-H_{29}, H_{27}-C_{26}-H_{29}, H_{27}-C_{26}-H_{28}
90–92	β_i	C-C-H (Methyl 2)	C_{23}-C_{26}-H_{27}, C_{23}-C_{26}-H_{28}, C_{23}-C_{26}-H_{29}
93–94	ϕ_i	N-C-C (Ring 2)	N_{22}-C_{30}-C_{31}, N_{22}-C_{30}-C_{35}
95–100	δ_i	C-C-C (Ring 2)	C_{31}-C_{30}-C_{35}, C_{30}-C_{31}-C_{32}, C_{31}-C_{32}-C_{33}, C_{32}-C_{33}-C_{34}, C_{33}-C_{34}-C_{35}, C_{30}-C_{35}-C_{34}
101–110	θ_i	H-C-C (Ring 2)	H_{36}-C_{35}-C_{30}, H_{36}-C_{35}-C_{34}, H_{37}-C_{34}-C_{35}, H_{37}-C_{34}-C_{33}, H_{38}-C_{33}-C_{34}, H_{38}-C_{33}-C_{32}, H_{39}-C_{32}-C_{33}, H_{39}-C_{32}-C_{31}, H_{40}-C_{31}-C_{32}, H_{40}-C_{31}-C_{30}
Out-of-plane bending (wagging)			
111–115	ω_i	C-H (ring 1)	H_7-C_6-C_1-C_5, H_8-C_1-C_2-C_6, H_9-C_2-C_1-C_3, H_{10}-C_3-C_2-C_4, H_{11}-C_4-C_3-C_5

No.	Symbol	Type	Definition
116	ω_i	C-N (ring 1)	N_{12}-C_5-C_4-C_6
117	ω_i	N-C (ring 1)	C_5-N_{12}-C_{13}-C_{20}
118	ω_i	C-O (urea)	O_{21}-C_{20}-N_{12}-N_{22}
119	ω_i	N-C (ring 2)	C_{20}-N_{22}-C_{30}-C_{23}
120	ω_i	C-N (ring 2)	N_{22}-C_{30}-C_{31}-C_{35}
121–125	ω_i	C-H (ring 2)	H_{36}-C_{35}-C_{34}-C_{30}, H_{37}-C_{34}-C_{33}-C_{35}, H_{38}-C_{33}-C_{32}-C_{34}, H_{39}-C_{32}-C_{31}-C_{33}, H_{40}-C_{31}-C_{30}-C_{32}
Torsion			
126–131	τ_i	C-C (ring 1)	C_6-C_1-C_2-C_3, C_1-C_2-C_3-C_4, C_2-C_3-C_4-C_5, C_3-C_4-C_5-C_6, C_4-C_5-C_6-C_1, C_5-C_6-C_1-C_2
132–135	τ_i	C-N (chain)	C_4-C_5-N_{12}-C_{13}, C_4-C_5-N_{12}-C_{20}, C_6-C_5-N_{12}-C_{13}, C_6-C_5-N_{12}-C_{20}
136–141	τ_i	N-C (methylene 1)	C_5-N_{12}-C_{13}-H_{14}, C_5-N_{12}-C_{13}-H_{15}, C_5-N_{12}-C_{13}-C_{16}, C_{20}-N_{12}-C_{13}-H_{14}, C_{20}-N_{12}-C_{13}-H_{15}, C_{20}-N_{12}-C_{13}-C_{16}
142–150	τ_i	C-C (methyl 1)	N_{12}-C_{13}-C_{16}-H_{17}, N_{12}-C_{13}-C_{16}-H_{18}, N_{12}-C_{13}-C_{16}-H_{19}, H_{14}-C_{13}-C_{16}-H_{17}, H_{14}-C_{13}-C_{16}-H_{18}, H_{14}-C_{13}-C_{16}-H_{19}, H_{15}-C_{13}-C_{16}-H_{17}, H_{15}-C_{13}-C_{16}-H_{18}, H_{15}-C_{13}-C_{16}-H_{19}
151–154	τ_i	N-C (urea)	C_5-N_{12}-C_{20}-O_{21}, C_5-N_{12}-C_{20}-N_{22}, C_{13}-N_{12}-C_{20}-O_{21}, C_{13}-N_{12}-C_{20}-N_{22}
155–158	τ_i	C-N (urea)	O_{21}-C_{20}-N_{22}-C_{30}, O_{21}-C_{20}-N_{22}-C_{23}, N_{12}-C_{20}-N_{22}-C_{30}, N_{12}-C_{20}-N_{22}-C_{23}
159–164	τ_i	N-C (methylene 2)	C_{20}-N_{22}-C_{23}-H_{24}, C_{20}-N_{22}-C_{23}-H_{25}, C_{20}-N_{22}-C_{23}-C_{26}, C_{30}-N_{22}-C_{23}-H_{24}, C_{30}-N_{22}-C_{23}-H_{25}, C_{30}-N_{22}-C_{23}-C_{26}
165–173	τ_i	C-C (methyl 2)	N_{22}-C_{23}-C_{26}-H_{27}, N_{22}-C_{23}-C_{26}-H_{28}, N_{22}-C_{23}-C_{26}-H_{29}, H_{24}-C_{23}-C_{26}-H_{27}, H_{24}-C_{23}-C_{26}-H_{28}, H_{24}-C_{23}-C_{26}-H_{29}, H_{25}-C_{23}-C_{26}-H_{27}, H_{25}-C_{23}-C_{26}-H_{28}, H_{25}-C_{23}-C_{26}-H_{29}
174–179	τ_i	C-C (ring 2)	C_{35}-C_{30}-C_{31}-C_{32}, C_{30}-C_{31}-C_{32}-C_{33}, C_{31}-C_{32}-C_{33}-C_{34}, C_{32}-C_{33}-C_{34}-C_{35}, C_{33}-C_{34}-C_{35}-C_{30}, C_{34}-C_{35}-C_{30}-C_{31}
180–183	τ_i	C-N (chain)	C_{31}-C_{30}-N_{22}-C_{20}, C_{31}-C_{30}-N_{22}-C_{23}, C_{35}-C_{30}-N_{22}-C_{20}, C_{35}-C_{30}-N_{22}-C_{23}

8.4.1 Phenyl ring vibrations

The vibrational modes of monosubstituted phenyl rings (Ph1 and Ph2) have been studied according to Wilson's numbering convention [99]. The selection rule for monosubstituted benzene rings allow five C−C stretching modes: 8a, 8b, 19a, 19b and

14. The strong intense bands at 1598 cm^{-1} in IR and 1593 cm^{-1} in Raman are assigned to 8a mode. This 8a mode is obtained at 1600 cm^{-1} in the simulated spectra. Normal coordinate analysis results predict that a band at 1535 cm^{-1} is due to the mode 8b and it is 1530 cm^{-1} in experimental IR spectrum. The mode 19a and 19b is expected in the region 1515 − 1470 cm^{-1} and 1470 − 1440 cm^{-1} [99] respectively. The mode 19a is observed as strong band at 1492 cm^{-1} in IR. The shoulder band at 1312 cm^{-1} in IR is assigned to mode 14. The C-H stretching vibrations of monosubstituted benzene rings are expected in the region 3120 − 3010 cm^{-1} [99]. The modes 2, 7a, 7b, 20a and 20b are classified as the C-H stretching modes of substituted phenyl rings. The strong intense band in IR at 3086 cm^{-1} is assigned as 20a mode of phenyl rings Ph1 and Ph2. The mode 2 is active in both IR and Raman as a strong intense band at 3060 cm^{-1}. The band observed at 3035 cm^{-1} in IR has been identified as mode 20b. The normal modes 3, 9a, 15, 18a and 18b are attributed as the C-H in plane bending vibrations of monosubstituted phenyl ring. The mode 3 appears in the region 1331 − 1253 cm^{-1}. The band at 1312 cm^{-1} in IR is assigned to mode 3 and this mode couples with mode 14. The strong band observed at 1169 cm^{-1} in IR and medium intense band at 1170 cm^{-1} in Raman is due to 9a mode. Mode 15 of both the phenyl rings is observed as medium intense band at 1155 cm^{-1} in the Raman spectrum. The modes 18a and 18b appears in the region 1032 − 1019 cm^{-1} and 1082 − 1065 cm^{-1} respectively. Strong bands at 1022 cm^{-1} (IR) and 1026 cm^{-1} (Raman) have been assigned to mode 18a.

Table 8.5 Definition of local symmetry coordinates (much like the natural internal coordinates) and the corresponding force constant (mdyne/A°) of EC with scale factors used.

No.	Symbol	Definition	Scale factors	Force constants (mdyne/Å)
		Stretching		
1–6	Ph1[νCC]	R_1, R_2, R_3, R_4, R_5, R_6	0.95313	6.508
7–11	Ph1[νCH]	r_7, r_8, r_9, r_{10}, r_{11}	0.91698	5.132
12	Ph1[νCN]	P_{12}	1.11245	6.199
13	Ph1[νNC]	P_{13}	0.82436	3.995
14	Mn1[CH_{2ss}]	$(r_{14}+r_{15})/\sqrt{2}$	0.91846	4.945
15	Mn1[CH_{2ips}]	$(r_{14}-r_{15})/\sqrt{2}$	0.86123	4.561
16	Mn1[νCC]	r_{16}	0.97979	4.284
17	Me1[CH_{3ss}]	$(r_{17}+r_{18}+r_{19})/\sqrt{3}$	0.88267	4.775
18	Me1[CH_{3ips}]	$(2r_{17}-r_{18}-r_{19})/\sqrt{6}$	0.89340	4.715
19	Me1[CH_{3ops}]	$(r_{18}-r_{19})/\sqrt{2}$	0.88733	4.710
20	ν(C=O)	Q_{20}	0.90769	10.858
21	CN_{ss}	$(r_{21}+r_{22})/\sqrt{2}$	1.09328	7.511
22	CN_{ips}	$(r_{21}-r_{22})/\sqrt{2}$	0.89652	4.863
23	Ph2[νNC]	P_{23}	0.86821	4.208
24	Mn2[CH_{2ss}]	$(r_{24}+r_{25})/\sqrt{2}$	0.91755	4.941
25	Mn2[CH_{2ips}]	$(r_{24}-r_{25})/\sqrt{2}$	0.86123	4.561
26	Mn2[νCC]	R_{26}	0.97979	4.284
27	Me2[CH_{3ss}]	$(r_{27}+r_{28}+r_{29})/\sqrt{3}$	0.88250	4.774
28	Me2[CH_{3ips}]	$(2r_{27}-r_{28}-r_{29})/\sqrt{6}$	0.89081	4.755
29	Me2[CH_{3ops}]	$(r_{28}-r_{29})/\sqrt{2}$	0.89017	4.671
30	Ph2[νCN]	P_{30}	1.01669	5.666
31–36	Ph2[νCC]	R_{31}, R_{32}, R_{33}, R_{34}, R_{35}, R_{36}	0.95313	6.508
37–41	Ph2[νCH]	r_{37}, r_{38}, r_{39}, r_{40}, r_{41}	0.91698	5.132
		Bending		
42	$Ph1_{trid}$	$(\delta_{42}-\delta_{43}+\delta_{44}-\delta_{45}+\delta_{46}-\delta_{47})/\sqrt{6}$	0.87628	1.151
43	$Ph1_{asyd}$	$(2\delta_{42}-\delta_{43}-\delta_{44}+2\delta_{45}-\delta_{46}-\delta_{47})/\sqrt{6}$	1.08408	1.411
44	$Ph1_{asydo}$	$(\delta_{43}-\delta_{44}+\delta_{46}-\delta_{47})/2$	0.77967	1.052

No.	Symbol	Definition	Scale factors	Force constants (mdyne/Å)
45–49	Ph1[δCH]	$(\theta_{48}-\theta_{49})/\sqrt{2}$, $(\theta_{50}-\theta_{51})/\sqrt{2}$, $(\theta_{52}-\theta_{53})/\sqrt{2}$, $(\theta_{54}-\theta_{55})/\sqrt{2}$, $(\theta_{56}-\theta_{57})/\sqrt{2}$	0.88992	0.478
50	Ph1[δCN]	$(\phi_{58}-\phi_{59})/\sqrt{2}$	0.31312	0.324
51	Ph1[NC_{roc}]	$(\beta_{60}-\beta_{61})/\sqrt{2}$	1.11722	1.212
52	Ph1[δCNC]	$(2\alpha_{62}-\beta_{60}-\beta_{61})/\sqrt{6}$	0.96914	1.248
53	Mn1[CH_{2sci}]	$(5\alpha_{63}+\gamma_{64})/\sqrt{26}$	0.91565	0.780
54	Mn1[CNC_{sci}]	$(\alpha_{63}+5\gamma_{64})/\sqrt{26}$	1.04414	1.579
55	Mn1[CH_{2roc}]	$(\beta_{65}-\beta_{66}+\beta_{67}-\beta_{68})/\sqrt{4}$	0.99431	0.966
56	Mn1[CH_{2wag}]	$(\beta_{65}+\beta_{66}-\beta_{67}-\beta_{68})/\sqrt{4}$	0.90643	0.693
57	Mn1[CH_{2twi}]	$(\beta_{65}-\beta_{66}-\beta_{67}+\beta_{68})/\sqrt{4}$	0.85811	0.639
58	Me1[CH_{3sd}]	$(\alpha_{69}+\alpha_{70}+\alpha_{71}-\beta_{72}-\beta_{73}-\beta_{74})/\sqrt{6}$	0.93422	0.556
59	Me1[CH_{3ipb}]	$(2\alpha_{69}-\alpha_{70}-\alpha_{71})/\sqrt{6}$	0.88592	0.538
60	Me1[CH_{3opb}]	$(\alpha_{70}-\alpha_{71})/\sqrt{2}$	0.91638	0.558
61	Me1[CH_{3ipr}]	$(2\beta_{72}-\beta_{73}-\beta_{74})/\sqrt{6}$	0.83137	0.573
62	Me1[CH_{3opr}]	$(\beta_{73}-\beta_{74})/\sqrt{2}$	0.87364	0.587
63	CN_{sd}	$(2\alpha_{75}-\beta_{76}-\beta_{77})/\sqrt{6}$	0.77122	1.233
64	CN_{roc}	$(\beta_{76}-\beta_{77})/\sqrt{2}$	1.12932	1.659
65	Ph2[NC_{roc}]	$(\beta_{78}-\beta_{79})/\sqrt{2}$	1.11722	1.227
66	Ph2[δCNC]	$(2\alpha_{80}-\beta_{78}-\beta_{79})/\sqrt{6}$	0.87476	1.078
67	Mn2[CH_{2sci}]	$(5\alpha_{81}+\gamma_{82})/\sqrt{26}$	0.91565	0.780
68	Mn2[NCC_{sci}]	$(\alpha_{81}+5\gamma_{82})/\sqrt{26}$	1.04414	1.579
69	Mn2[CH_{2roc}]	$(\beta_{83}-\beta_{84}+\beta_{85}-\beta_{86})/\sqrt{4}$	0.99431	0.965
70	Mn2[CH_{2wag}]	$(\beta_{83}+\beta_{84}-\beta_{85}-\beta_{86})/\sqrt{4}$	0.90643	0.693
71	Mn2[CH_{2twi}]	$(\beta_{83}-\beta_{84}-\beta_{85}+\beta_{86})/\sqrt{4}$	0.85811	0.639
72	Me2[CH_{3sd}]	$(\alpha_{87}+\alpha_{88}+\alpha_{89}-\beta_{90}-\beta_{91}-\beta_{92})/\sqrt{6}$	0.93422	0.556
73	Me2[CH_{3ipb}]	$(2\alpha_{87}-\alpha_{88}-\alpha_{89})/\sqrt{6}$	0.90212	0.543
74	Me2[CH_{3opb}]	$(\alpha_{88}-\alpha_{89})/\sqrt{2}$	0.99044	0.609
75	Me2[CH_{3ipr}]	$(2\beta_{90}-\beta_{91}-\beta_{92})/\sqrt{6}$	1.04175	0.713
76	Me2[CH_{3opr}]	$(\beta_{91}-\beta_{92})/\sqrt{2}$	0.80865	0.548
77	Ph2[δCN]	$(\phi_{93}-\phi_{94})/\sqrt{2}$	0.31312	0.324
78	$Ph2_{trid}$	$(\delta_{95}-\delta_{96}+\delta_{97}-\delta_{98}+\delta_{99}-\delta_{100})/\sqrt{6}$	0.92968	1.221
79	$Ph2_{asyd}$	$(2\delta_{95}-\delta_{96}-\delta_{97}+2\delta_{98}-\delta_{99}-\delta_{100})/\sqrt{6}$	0.97769	1.340

No.	Symbol	Definition	Scale factors	Force constants (mdyne/Å)
80	$Ph2_{asydo}$	$(\delta_{96}-\delta_{97}+\delta_{99}-\delta_{100})/2$	0.49708	0.636
81–85	Ph2[δCH]	$(\theta_{101}-\theta_{102})/\sqrt{2}$, $(\theta_{103}-\theta_{104})/\sqrt{2}$, $(\theta_{105}-\theta_{106})/\sqrt{2}$, $(\theta_{107}-\theta_{108})/\sqrt{2}$, $(\theta_{109}-\theta_{110})/\sqrt{2}$	0.88992	0.478
Out-of-plane bending (wagging)				
86–90	Ph1[gCH]	ω_{111}, ω_{112}, ω_{113}, ω_{114}, ω_{115}	0.90813	0.407
91	Ph1[gCN]	ω_{116}	1.18012	0.796
92	Ph1[gNC]	ω_{117}	1.19820	0.321
93	gCO	ω_{118}	0.84948	0.632
94	Ph2[gNC]	ω_{119}	1.19820	0.316
95	Ph2[gCN]	ω_{120}	1.18012	0.796
96–100	Ph2[gCH]	ω_{121}, ω_{122}, ω_{123}, ω_{124}, ω_{125}	0.90813	0.407
Torsion				
101	$Ph1_{puck}$	$(\tau_{126}-\tau_{127}+\tau_{128}-\tau_{129}+\tau_{130}-\tau_{131})/\sqrt{6}$	0.87610	0.350
102	$Ph1_{asyt}$	$(\tau_{126}-\tau_{128}+\tau_{129}-\tau_{131})/2$	1.18182	0.408
103	$Ph1_{asyto}$	$(-\tau_{126}+2\tau_{127}-\tau_{128}-\tau_{129}+2\tau_{130}-\tau_{131})/\sqrt{12}$	0.78677	0.265
104	Ph1[τCN]	$(\tau_{132}+\tau_{133}+\tau_{134}+\tau_{135})/2$	1.02194	0.047
105	Mn1[τCH_2]	$(\tau_{136}+\tau_{137}+\tau_{138}+\tau_{139}+\tau_{140}+\tau_{141})/\sqrt{6}$	1.24724	0.035
106	Me1[τCH_3]	$(\tau_{142}+\tau_{143}+\tau_{144}+\tau_{145}+\tau_{146}+\tau_{147}+\tau_{148}+\tau_{149}+\tau_{150})/3$	0.94491	0.012
107	τNC	$(\tau_{151}+\tau_{152}+\tau_{153}+\tau_{154})/2$	0.77626	0.093
108	τCN	$(\tau_{155}+\tau_{156}+\tau_{157}+\tau_{158})/2$	0.77626	0.093
109	Mn2[τCH_2]	$(\tau_{159}+\tau_{160}+\tau_{161}+\tau_{162}+\tau_{163}+\tau_{164})/\sqrt{6}$	1.24724	0.035
110	Me2[τCH_3]	$(\tau_{165}+\tau_{166}+\tau_{167}+\tau_{168}+\tau_{169}+\tau_{170}+\tau_{171}+\tau_{172}+\tau_{173})/3$	0.94491	0.012
111	$Ph2_{puck}$	$(\tau_{174}-\tau_{175}+\tau_{176}-\tau_{177}+\tau_{178}-\tau_{179})/\sqrt{6}$	1.03926	6.427
112	$Ph2_{asyt}$	$(\tau_{174}-\tau_{176}+\tau_{177}-\tau_{179})/2$	0.63669	0.212
113	$Ph2_{asyto}$	$(-\tau_{174}+2\tau_{175}-\tau_{176}-\tau_{177}+2\tau_{178}-\tau_{179})/\sqrt{12}$	0.94870	4.987
114	Ph2[τCN]	$(\tau_{180}+\tau_{181}+\tau_{182}+\tau_{183})/2$	1.02194	0.047

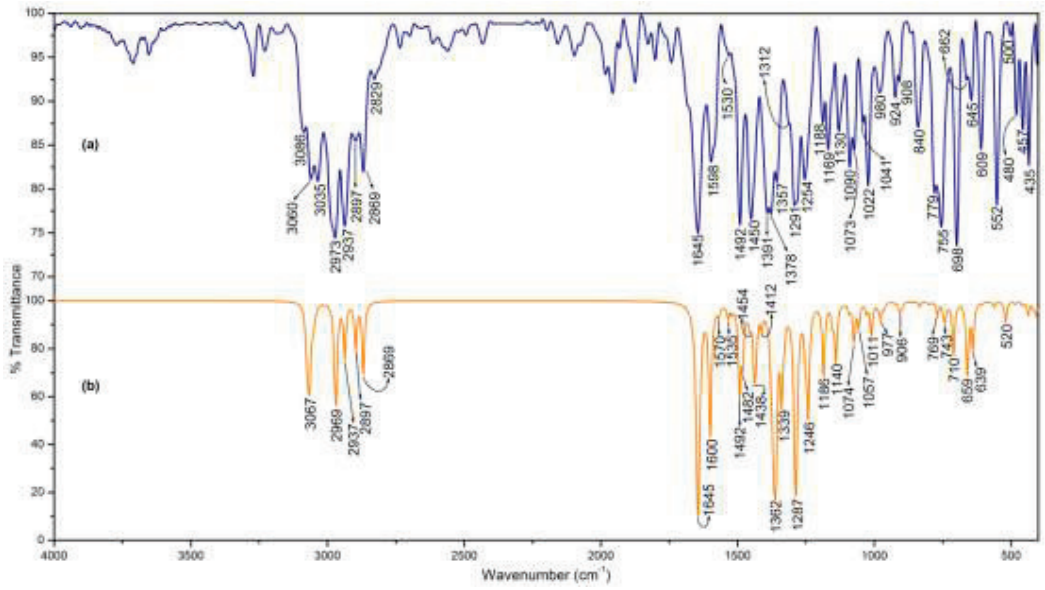

Fig. 8.2 (a) Experimental and (b) simulated IR spectra of ethyl centralite.

8.4.2 Ethyl group vibrations

Ethyl centralite consists of two ethyl groups connected by the urea moiety. Vibrational analysis of ethyl group is the normal mode vibrations of methyl (Me1 and Me2) and methylene (Mn1 and Mn2) groups. The asymmetric and symmetric stretching modes of methyl group were expected in the region 2972 − 2952 cm^{-1} and 2882 − 2862 cm^{-1} [30] respectively. The asymmetric stretching (in-plane stretching) mode is observed as a strong intense band at 2973 cm^{-1} in IR and as a medium intense band at 2975 cm^{-1} in Raman spectra. The out-of-plane stretching mode manifests as very intense bands in the IR and Raman spectra at 2937 cm^{-1}. The symmetric stretching vibration of two methyl groups is observed at 2869 cm^{-1} as strong band in IR and weak band in Raman spectra. Methyl symmetric and asymmetric deformation vibrations are expected in the region 1380 − 1370 cm^{-1} and 1470 − 1440 cm^{-1} [30], which are 1378 cm^{-1} and 1450 cm^{-1} in Raman spectrum respectively. Methyl rocking generally appears as a weak, moderate or sometimes strong band in the regions

1080−1020 cm^{-1} and 1020−930 cm^{-1} [100], which are observed at 1073 cm^{-1} in IR and 1076 cm^{-1} in Raman. Methyl rocking vibration is obtained at 1074 cm^{-1} in the simulated spectra. The medium intense band observed at 297 cm^{-1} in Raman spectrum is due to torsion vibration of methyl group.

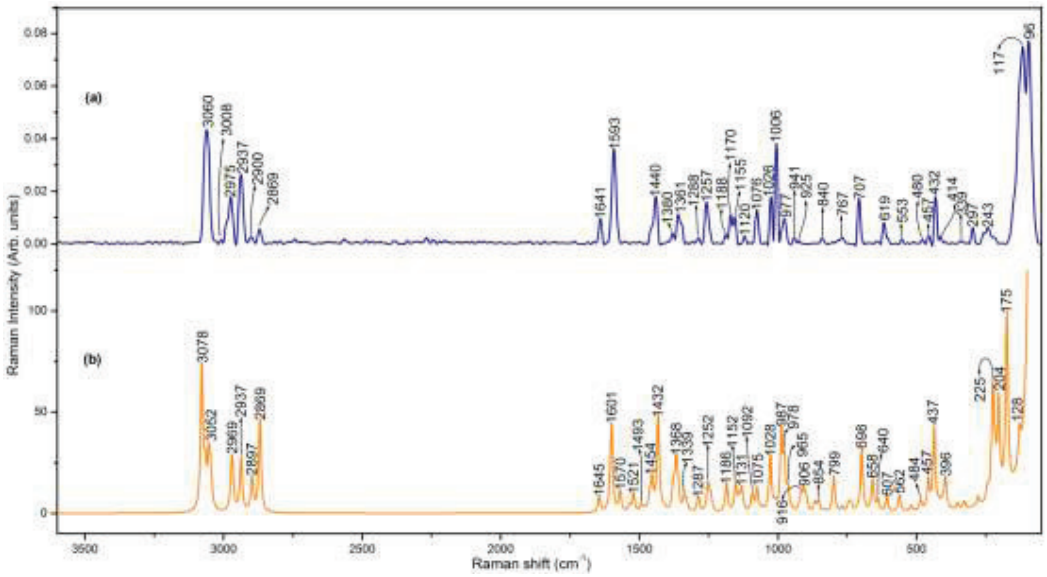

Fig. 8.3 (a) Experimental and (b) simulated Raman spectra of ethyl centralite.

The methylene asymmetric and symmetric stretching vibrations are expected in the region 2936 − 2916 cm^{-1} and 2865 − 2845 cm^{-1} [101] respectively. NCA predicts that medium intense IR band at 2897 cm^{-1} and weak band at 2900 cm^{-1} in Raman spectrum is due to asymmetric CH_2 stretching mode. The medium intense band at 1440 cm^{-1} in Raman spectrum corresponds to scissoring modes of methylene (Mn1 and Mn2) groups. This vibration is found in the expected range 1480 − 1440 cm^{-1} [103]. Methylene wagging modes are expected in the region 1411 − 1174 cm^{-1} [158]. The sharp band at 1357 cm^{-1} in IR and 1361 cm^{-1} in Raman is assigned to methylene wagging mode. The band at 1254 cm^{-1} in IR and 1257 cm^{-1} in Raman spectra is identified as CH_2 twisting mode. The CH_2 rocking mode appears as a strong

intense band at 1130 cm^{-1} in IR and as weak band at 1120 cm^{-1} in Raman spectra. In the present study, the methylene bending modes follow an order in decreasing wavenumber which is CH_2 scissoring > CH_2 wagging > CH_2 twisting > CH_2 rocking.

Table 8.6 Vibrational assignment of ethyl centralite by normal coordinate analysis based on SQM force field calculations.

Calculated {B3LYP/6-31G(d)}				Observed (cm^{-1})		Assignment (% PED, internal coordinates having contribution ≥ 10% are shown)
$\nu_{Unscaled}$ (cm^{-1})	ν_{Scaled} (cm^{-1})	IR intensity (%)	Raman intensity (%)	ν_{IR}	ν_{Raman}	
3214	3078	1.86	3.51	3086	-	Ph2[νCH(64)] + Ph1[νCH(35)]
3214	3078	1.08	0.41	3086	-	Ph1[νCH(64)] + Ph2[νCH(35)]
3210	3073	8.19	0.02	-	-	Ph1[νCH(74)] + Ph2[νCH(26)]
3209	3072	3.76	0.04	-	-	Ph2[νCH(74)] + Ph1[νCH(26)]
3203	3066	9.36	0.45	3060	3060	Ph2[νCH(86)] + Ph1[νCH(14)]
3202	3066	7.15	0.49	-	-	Ph1[νCH(86)] + Ph2[νCH(14)]
3191	3054	2.47	0.85	-	-	Ph1[νCH(99)]
3191	3051	1.97	0.87	-	-	Ph2[νCH(99)]
3183	3045	0.46	0.3	-	-	Ph2[νCH(99)]
3182	3044	0.46	0.28	3035		Ph1[νCH(99)]
3155	2973	4.77	0.15	2973	2975	Me2[CH_{3ips}(71)] + Me1[CH_{3ips}(12)]
3155	2973	4.55	0.28	2973	2975	Me1[CH_{3ips}(37)] + Me1[CH_{3ops}(30)] + Me2[CH_{3ips}(24)]
3139	2969	9.54	0.67	-	-	Mn1[CH_{2ss}(79)] + Me1[CH_{3ops}(12)]
3139	2968	9.87	0.64	-	-	Mn2[CH_{2ss}(81)] + Mn2[CH_{2ips}(12)]
3116	2937	7.13	0.57	2937	2937	Me1[CH_{3ips}(38)] + Me1[CH_{3ops}(32)] + Me2[CH_{3ops}(22)]
3116	2937	4.25	0.92	2937	2937	Me2[CH_{3ops}(69)] + Me1[CH_{3ips}(12)] + Me1[CH_{3ops}(10)]

Calculated {B3LYP/6-31G(d)}				Observed (cm^{-1})		Assignment (% PED, internal coordinates having contribution ≥ 10% are shown)
$\nu_{Unscaled}$ (cm^{-1})	ν_{Scaled} (cm^{-1})	IR intensity (%)	Raman intensity (%)	ν_{IR}	ν_{Raman}	
3079	2897	2.55	0.57	2897	2900	Mn1[CH_{2ips}(52)] + Mn2[CH_{2ips}(33)]
3079	2897	6.77	0.39	2897	2900	Mn2[CH_{2ips}(52)] + Mn1[CH_{2ips}(33)]
3055	2869	3.62	2.06	2869	2869	Me1[CH_{3ss}(71)] + Me2[CH_{3ss}(24)]
3055	2869	11.98	0.49	2869	2869	Me2[CH_{3ss}(71)] + Me1[CH_{3ss}(24)]
1735	1645	100	0.48	1645	1641	ν(C=O)(65) + CN_{ss}(16)
1658	1602	6.27	1.4	1598	1593	Ph2[νCC(59)] + Ph2[δCH(15)]
1658	1600	29.43	1.11	1598	1593	Ph1[νCC(56)] + Ph1[δCH(14)]
1641	1569	1.79	0.59	-	-	Ph1[νCC(71)] + Ph1[δCH(18)]
1640	1535	2.37	0.17	1530	-	Ph2[νCC(74)] + Ph2[δCH(21)]
1546	1521	1.32	0.53	-	-	Me2[CH_{3opb}(95)]
1544	1493	20.18	0.21	1492	-	Ph1[δCH(38)] + Ph1[νCC(34)] + Ph1[νCN(17)]
1539	1481	11.67	0.07	-	-	Ph2[δCH(45)] + Ph2[νCC(35)] + Ph2[νCN(11)]
1539	1463	0.91	0.37	-	-	Me1[CH_{3opb}(76)] + Me1[CH_{3ipb}(10)]
1521	1454	3.22	0.86	1450	-	Me2[CH_{3ipb}(81)] + Me2[CH_{3ipr}(12)]
1520	1439	13.52	0.03	-	1440	Mn2[CH_{2sci}(42)] + Mn1[CH_{2sci}(38)]
1506	1434	4.24	1.03	-	-	Me1[CH_{3ipb}(78)]
1502	1431	4.2	1.73	-	-	Mn1[CH_{2sci}(45)] + Mn2[CH_{2sci}(42)]
1500	1413	2.93	0.04	-	-	Ph1[δCH(50)] + Ph1[νCC(37)]
1498	1411	0.8	0.05	1391	-	Ph2[δCH(48)] + Ph2[νCC(39)]
1433	1378	3.15	0.39	1378	1380	Me2[CH_{3sd}(70)]
1433	1378	3.56	0.22	1378	1380	Me1[CH_{3sd}(70)]
1422	1368	41.6	1.27	-	-	Ph1[νCN(18)] +

Calculated {B3LYP/6-31G(d)}				Observed (cm^{-1})		Assignment (% PED, internal coordinates having contribution ≥ 10% are shown)
$\nu_{Unscaled}$ (cm^{-1})	ν_{Scaled} (cm^{-1})	IR intensity (%)	Raman intensity (%)	ν_{IR}	ν_{Raman}	
						CN_{ips}(16) + Mn1[CH_{2twi}(13)]
1410	1361	58.69	0.64	1357	1361	CN_{ips}(23) + Mn1[CH_{2wag}(15)]
1405	1339	20.41	0.34	-	-	Mn2[CH_{2wag}(33)] + Ph2[νCN(14)] + Mn2[CH_{2twi}(11)]
1395	1330	3.13	0.28	-	-	Mn1[CH_{2wag}(46)] + Mn2[CH_{2wag}(29)]
1365	1290	9.65	0.02	-	-	Ph2[νCC(36)] + Ph1[νCC(22)] + Ph2[δCH(20)] + Ph1[δCH(14)]
1363	1289	3.45	0.08	1312	-	Ph1[νCC(49)] + Ph2[νCC(19)] + Ph1[δCH(17)] + Ph2[δCH(10)]
1343	1287	63.25	0.37	1291	1288	Ph2[νCC(21)] + CN_{roc}(11)
1337	1253	4.64	0.65	-	-	Mn2[CH_{2twi}(31)] + Me2[CH_{3ipr}(15)] + Ph2[νCN(13)]
1318	1250	3.91	0.16	-	-	Ph1[νCC(22)] + Ph1[δCH(20)] + Ph2[νCC(19)] + Ph2[δCH(13)]
1298	1242	1.45	0.25	-	-	Ph1[νCC(30)] + Mn1[CH_{2twi}(21)] + Ph1[δCH(19)]
1286	1242	25.3	0.18	1254	1257	Ph2[νCC(31)] + Ph2[δCH(22)] + Mn1[CH_{2twi}(18)]
1218	1186	15.94	0.82	1188	1188	Ph2[νNC(10)]
1208	1153	1.87	0.29	1169	1170	Ph1[δCH(50)] + Ph2[δCH(29)] + Ph1[νCC(10)]
1207	1152	1.65	0.46	-	1155	Ph2[δCH(51)] + Ph1[δCH(28)] + Ph2[νCC(10)]
1192	1140	12.04	0.31	1130	1120	Mn1[CH_{2roc}(16)] + Mn2[CH_{2roc}(10)]
1192	1130	0.07	0.34	-	-	Ph1[δCH(55)] +

Calculated {B3LYP/6-31G(d)}				Observed (cm^{-1})		Assignment (% PED, internal coordinates having contribution ≥ 10% are shown)
$\nu_{Unscaled}$ (cm^{-1})	ν_{Scaled} (cm^{-1})	IR intensity (%)	Raman intensity (%)	ν_{IR}	ν_{Raman}	
						Ph2[δCH(34)]
1165	1130	0.02	0.3	-	-	Ph2[δCH(56)] + Ph1[δCH(34)]
1150	1093	1.47	0.5	1090	-	Ph2[νNC(16)] + Ph1[νNC(12)] + Mn1[CH_{2roc}(10)]
1123	1076	3.34	0.45	-	-	Mn1[νCC(35)] + Me1[CH_{3opr}(29)] + Mn1[CNC_{sci}(15)] + Me1[CH_{3ipr}(10)]
1112	1074	4.84	0.23	1073	1076	Me2[CH_{3opr}(33)] + Mn2[νCC(29)] + Mn2[NCC_{sci}(14)]
1111	1057	3.86	0.03	-	-	Ph1[νCC(35)] + Ph1[δCH(31)] + Ph2[νCC(15)] + Ph2[δCH(13)]
1105	1057	0.63	0.06	1041	-	Ph2[νCC(36)] + Ph2[δCH(31)] + Ph1[νCC(15)] + Ph1[δCH(13)]
1066	1028	0.44	0.22	1022	1026	Ph2[νCC(39)] + Ph1[νCC(21)] + Ph2[δCH(17)]
1058	1028	1.37	1.34	-	-	Ph1[νCC(45)] + Ph2[νCC(24)] + Ph1[δCH(18)]
1052	1011	6.49	0.18	-	1006	Ph1[νNC(18)] + Ph2[νNC(18)] + Mn2[νCC(15)] + Mn1[νCC(13)]
1019	988	0.84	2.07	980	977	$Ph2_{trid}$(63) + Ph2[νCC(31)]
1019	977	3.01	1.25	-	-	Ph1[νCC(27)] + CN_{ss}(10) + $Ph1_{trid}$(10) + $Ph2_{trid}$(10)
994	964	1.27	0.59	980	977	$Ph1_{trid}$(51) + Mn1[νCC(10)]
989	927	0.13	0.03	-	941	Ph1[gCH(86)]
988	926	0.03	0.05	-	-	$Ph2_{puck}$(42) + Ph2[gCH(30)] + $Ph2_{asyto}$(26)

Calculated {B3LYP/6-31G(d)}				Observed (cm^{-1})		Assignment (% PED, internal coordinates having contribution ≥ 10% are shown)
$\nu_{Unscaled}$ (cm^{-1})	ν_{Scaled} (cm^{-1})	IR intensity (%)	Raman intensity (%)	ν_{IR}	ν_{Raman}	
962	916	0.16	0.45	-	-	Mn2[νCC(10)]
961	907	1.35	0.33	-	-	Ph1[gCH(33)] + Ph2[gCH(25)]
956	906	0.51	0.17	924	925	Ph1[gCH(59)] + Ph2[gCH(14)]
941	898	1.05	0.35	908		Ph2[gCH(48)]
918	866	0.05	0.26	840	840	Ph1[gCH(53)]
918	854	0.11	0.31	840	840	Ph2[gCH(42)] + $Ph2_{puck}$(23) + $Ph2_{asyto}$(22)
856	834	0.96	0.06	-	-	Ph1[gCH(15)] + Ph2[gCH(13)]
849	803	0.23	0.05	-	-	Ph1[gCH(50)] + Ph2[gCH(49)]
845	799	0.31	0.96	-	-	Ph2[gCH(50)] + Ph1[gCH(48)]
793	769	2.41	0.13	779	-	Mn2[CH_{2roc}(36)] + Me2[CH_{3ipr}(14)] + Me2[CH_{3opr}(11)]
783	749	1.24	0.09	755	767	$Ph2_{puck}$(42) + $Ph2_{asyto}$(35)
778	743	3.06	0.19	-	-	Mn1[CH_{2roc}(26)] + Me1[CH_{3ipr}(15)] + Ph1[gCH(15)]
774	736	0.71	0.2	-	-	$Ph2_{puck}$(47) + $Ph2_{asyto}$(38)
763	710	10.88	0.05	-	707	gCO(54)
720	698	0.17	1.7	698	-	$Ph2_{asyd}$(20) + $Ph1_{asyd}$(11) + $Ph2_{puck}$(11)
711	660	12.73	0.44	662	-	$Ph2_{puck}$(50) + $Ph2_{asyto}$(39)
708	657	3.7	0.46	-	-	$Ph2_{puck}$(48) + $Ph2_{asyto}$(37)
657	639	9.2	0.32	645	-	$Ph2_{puck}$(44) + $Ph2_{asyto}$(34)
633	607	0.25	0.4	609	619	$Ph1_{asydo}$(26) + $Ph2_{puck}$(23) + $Ph2_{asyto}$(18) + $Ph1_{asyd}$(11)
631	562	1.12	0.47	552	553	$Ph2_{puck}$(53) +

Calculated {B3LYP/6-31G(d)}				Observed (cm^{-1})		Assignment (% PED, internal coordinates having contribution ≥ 10% are shown)
$\nu_{Unscaled}$ (cm^{-1})	ν_{Scaled} (cm^{-1})	IR intensity (%)	Raman intensity (%)	ν_{IR}	ν_{Raman}	
						$Ph2_{asyto}(37)$
610	520	3.95	0.16	500	-	$Ph2_{puck}(38)$ + $Ph2_{asyto}(24)$ + $Ph1_{puck}(18)$
559	485	0.49	0.28	480	480	$Ph2_{puck}(36)$ + $Ph2_{asyto}(21)$ + $Ph1_{asyt}(18)$
503	458	0.7	0.82	-	-	$Ph2_{asydo}(70)$
485	437	2.2	0.44	457	457	$Mn2[NCC_{sci}(18)]$ + $Ph2_{puck}(10)$ + Ph2[gNC(10)]
453	436	0.37	1.85	-	-	$Ph2_{puck}(14)$
434	419	0.99	0.14	-	414	$CN_{roc}(16)$ + $Ph1_{asyto}(12)$ + Ph1[δCNC(11)] + Ph1[gCH(10)] + $Ph1_{asyt}(10)$
429	407	2.5	0.22	435	432	$Mn1[CNC_{sci}(20)]$ + Ph1[gNC(10)]
423	396	1.12	0.88	405	-	$Ph1_{asyto}(23)$ + Ph1[gCH(14)]
421	352	0.87	0.15	-	-	$Ph1_{asyto}(12)$
396	328	0.12	0.2	-	339	Ph2[δCNC(17)] + $Me2[\tau CH_3(13)]$ + Ph1[δCNC(10)]
335	278	0.12	0.26	-	-	$Ph2_{asyto}(55)$ + $Ph2_{puck}(43)$
311	244	0.03	0.33	-	297	$Me1[\tau CH_3(18)]$ + $Ph1_{asyto}(12)$ + $Me2[\tau CH_3(11)]$
288	226	0.51	1.81	-	-	$Ph1_{asyto}(25)$ + $Me2[\tau CH_3(18)]$ + Ph1[gNC(12)] + Ph1[gCH(10)]
254	224	0.46	1.36	-	-	$Me1[\tau CH_3(18)]$ + Ph1[gNC(13)] + Ph1[δCN(12)] + $Me2[\tau CH_3(10)]$
240	216	0.1	0.66	-	-	$Me1[\tau CH_3(17)]$ + Ph1[δCNC(12)] + Ph1[δCN(11)]

Calculated {B3LYP/6-31G(d)}				Observed (cm^{-1})		Assignment (% PED, internal coordinates having contribution ≥ 10% are shown)
$\nu_{Unscaled}$ (cm^{-1})	ν_{Scaled} (cm^{-1})	IR intensity (%)	Raman intensity (%)	ν_{IR}	ν_{Raman}	
228	204	0.79	2.55	-	243	$Ph2_{asyt}$(21) + Ph2[gNC(19)] + Ph2[δCN(14)] + Ph2[gCH(10)]
205	175	0.1	4.9	-	-	$Ph2_{asyt}$(37) + Ph2[gCH(15)]
149	130	0.02	0.6	-	-	Ph2[δCN(21)] + Ph1[δCN(21)]
124	127	0.65	0.3	-	117	Mn2[τCH_2(15)] + Mn1[τCH_2(15)] + $Ph2_{asyto}$(11) + $Ph2_{puck}$(11) + Ph1[gNC(11)]
106	92	0.03	3.09	-	-	Mn1[τCH_2(41)] + Ph1[gNC(15)] + Ph2[gNC(10)]
84	91	0.01	3.9	-	-	Mn2[τCH_2(39)] + Ph2[gNC(10)] + Ph2[δCNC(10)]
84	87	0.36	20.45	-	96	$Ph2_{asyto}$(31) + $Ph2_{puck}$(29) + $Ph2_{asyt}$(10)
67	66	0.03	31.79	-	-	$Ph2_{asyto}$(40) + $Ph2_{puck}$(28) + Ph1[τCN(14)] + Ph2[τCN(11)]
62	59	0.04	71.34	-	-	$Ph2_{asyto}$(40) + $Ph2_{puck}$(33)
59	41	1.11	17.61	-	-	τNC(38) + τCN(37)
42	41	0.17	79.85	-	-	Ph2[τCN(29)] + Ph1[τCN(25)] + $Ph2_{asyt}$(11)
32	26	0	100	-	-	τCN(23) + τNC(22) + CN_{sd}(18)

Ph, phenyl ring (1, 2); Me, methyl (1, 2); Mn, methylene (1, 2); ν, stretching; δ, bending; τ, torsion; g, gauche; ss, symmetric stretching; ips, in plane stretching; ops, out of plane stretching; sd, symmetric deformation; ipb, in plane bending; opb, out of plane bending; ipr, in plane rocking; opr, out of plane rocking; puck, puckering; trid, trigonal deformation; asyd, asymmetric deformation; asydo, out of plane asymmetric deformation; asyt, asymmetric torsion; asyto, out of plane asymmetric torsion; sci, scissoring; roc, rocking; twi, twisting; wag, wagging.

8.4.3 Urea group vibrations

Vibrational analysis of urea moiety is made on the basis of carbonyl and C−N group vibrations. The band due to the stretching vibration of the carbonyl group of urea is expected around 1640 cm^{-1} [103]. The characteristic C=O stretching vibration occurs as a very sharp band at 1645 cm^{-1} in IR and exactly coincides with the calculated wavenumber. The Raman counterpart is observed at 1641 cm^{-1} with medium intensity. The bands observed at 1357 cm^{-1} in IR and 1361 cm^{-1} in Raman corresponds to the asymmetric CN stretching mode which is found coupled with the methylene wagging mode.

8.5 Electronic absorption spectra

The UV-visible spectrum of EC has been computed in the gas phase and the solvent effect is considered using time-dependent DFT and polarizable continuum model (PCM) [159-161] respectively. The experimental (ethanol) and simulated spectra (ethanol and gas phase) were shown in Fig. 8.4 and the results were presented in Table 8.7.

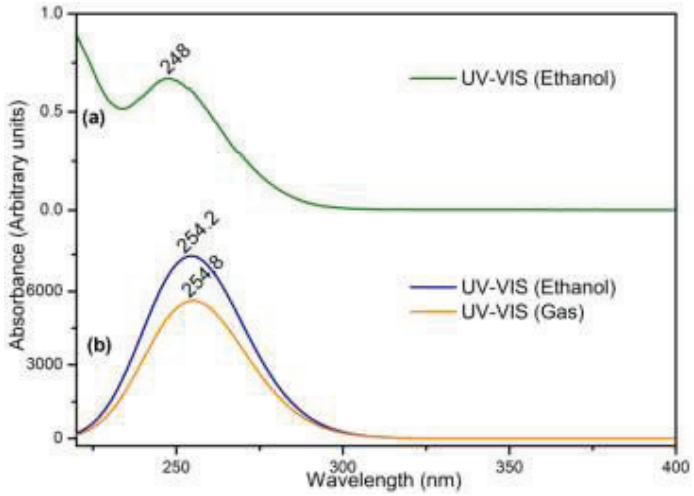

Fig. 8.4 (a) Experimental UV-visible spectrum of ethyl centralite in ethanol and (b) simulated UV-visible spectrum of ethyl centralite in gas phase and ethanol calculated using the PCM-TD-DFT method.

The highest occupied molecular orbital (HOMO) and the lowest unoccupied molecular orbital (LUMO) of EC has been calculated at the B3LYP/6-31G(d) level. The frontier molecular orbitals plot is shown in Fig. 8.5. The calculated energy of HOMO and LUMO orbitals are −5.829 and −0.283 eV respectively. The energy gap between HOMO and LUMO of EC molecule is found to be 5.546 eV.

Table 8.7 Experimental and calculated absorption wavelengths, energies, oscillator strengths of EC using TD-DFT method at the B3LYP/6-31G(d) level.

Phase	Experimental	Calculated			
	λ_{max} (nm)	λ_{max} (nm)	Energy (eV)	Oscillator strength	Composition (%)
Ethanol	248	256.60	4.8317	0.0463	H→L+1 (85%)
	-	256.15	4.8402	0.0752	H→L (93%)
	-	251.05	4.9386	0.0647	H→L+2 (84%)
Gas	-	257.48	4.8152	0.0207	H→L+1 (86%)
	-	257.46	4.8157	0.0573	H→L (92%)
	-	252.01	4.9197	0.0630	H→L+2 (84%)

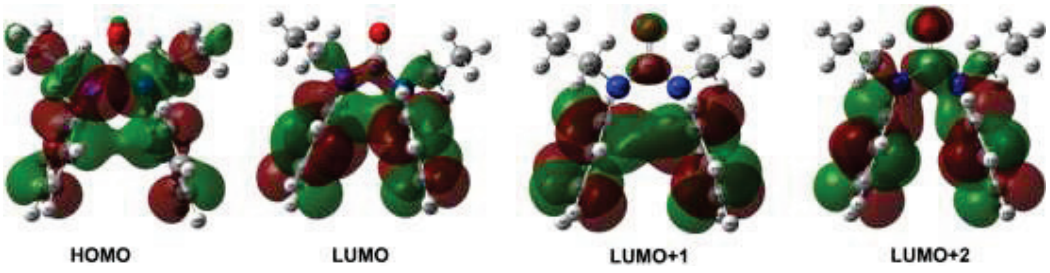

Fig. 8.5 Molecular frontier orbitals of ethyl centralite.

Electronic transitions corresponding to the electronic spectra of ethyl centralite is assigned to π→π* and n→π* electronic transitions. The LUMO has the electron density accumulated over the phenyl rings (Ph1, Ph2) whereas the HOMO has

electron density throughout the whole molecular skeleton. The HOMO→LUMO transition is regarded as π→π* transition yielding high oscillator strength 0.0752 in ethanol solvent. The HOMO→LUMO+1 clearly predict the charge transfer from lone pair nitrogen (N_{12}, N_{22}) to the phenyl rings showing the n→π* character. The transition HOMO→LUMO+2 show a sign of charge transfer from the lone pair nitrogen to the carbonyl group (C_{20}=O_{21}) and phenyl rings. The broad absorption band at 248 nm corresponds to H→L+1 transition.

8.6 Hyperpolarizability calculation

The first order hyperpolarizability of the ethyl centralite molecule has been computed using B3LYP/6-31G(d). The calculated total dipole moment, average polarizability and first hyperpolarizability of ethyl centralite were 1.176 Debye, 26.88 $\times 10^{-12}$ esu and 1.794 $\times 10^{-30}$ esu (which is 5 times that of urea) respectively. Hyperpolarizability β is the measure of non-linearity of the molecular system. Electron transfer through π conjugated framework from the donor to acceptor groups in the molecule can induce large variations of both the molecular dipole moment and the molecular polarizability enhancing IR and Raman activity at the same time. Simultaneous strong bands in both IR and Raman spectra are shown in Fig. 8.6. The bands at 1645, 1598, 1357, 1254, 1169, 1073, 1022, 980 cm^{-1} in FT-IR spectra and their counterparts at 1641, 1593, 1361, 1257, 1170, 1076, 1026, 977 cm^{-1} in FT-Raman spectra simultaneously have high intensities indicating non-linear optical activity of the compound.

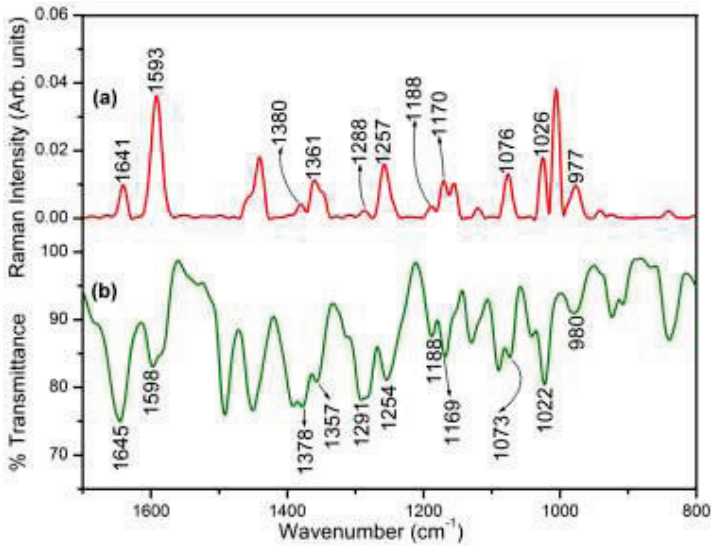

Fig. 8.6 Simultaneous strong bands both in (a) FT-Raman and (b) FT-IR spectra of ethyl centralite contributing to its NLO activity.

8.7 Conclusion

A density functional theoretical study on the molecular structure and spectral characteristics has been conducted on the organic compound ethyl centralite. The n→σ* interaction responsible for the distortion in the planarity of the phenyl rings and other energetic hyperconjugative interactions have been discussed in the natural orbital analysis. The frontier molecular orbitals plot revealed the charge transfer between the donor and acceptor groups. The HOMO-LUMO energy gap of the title compound is found to be 5.546 eV calculated by DFT. A complete assignment of experimental absorption peaks in the UV-Visible spectrum has been made by calculating the transition energies and oscillator strengths by time dependent density functional theory (TD-DFT). The calculated value of first order hyperpolarizability (β) of ethyl centralite have been found to be 1.794 $\times 10^{-30}$ esu which is five times than that of urea. The contribution of vibrational spectra in the non-linear optical activity of the molecule is discussed.